PHYSICAL REVIEW A **85**, 061605(R) (2012)

Magnetic phases of bosons with synthetic spin-orbit coupling in optical lattices

Zi Cai,[1] Xiangfa Zhou,[2] and Congjun Wu[1,3]

[1]*Department of Physics, University of California, San Diego, California 92093, USA*

[2]*Key Laboratory of Quantum Information, University of Science and Technology of China, CAS, Hefei, Anhui 230026, China*

[3]*Center for Quantum Information, IIIS, Tsinghua University, Beijing, China*

(Received 15 May 2012; published 20 June 2012)

We investigate magnetic properties in the superfluid and Mott-insulating states of two-component bosons with spin-orbit (SO) coupling in two-dimensional square optical lattices. The spin-independent hopping integral t and SO coupled one λ are fitted from band-structure calculations in the continuum, which exhibit oscillations with increasing SO coupling strength. The magnetic superexchange model is derived in the Mott-insulating state with one particle per site, characterized by the Dzyaloshinsky-Moriya interaction. In the limit of $|\lambda| \ll |t|$, we find a spin spiral Mott state whose pitch value is the same as that in the incommensurate superfluid state, while in the opposite limit $|t| \ll |\lambda|$, the ground state exhibits a 2×2 in-plane spin pattern.

DOI: 10.1103/PhysRevA.85.061605 PACS number(s): 67.85.Jk, 67.85.Hj, 05.30.Jp

Quantum many-body states with spontaneous incommensurate modulated structures have attracted considerable interest in the past decades, and occur in many settings of condensed matter and ultracold atom physics. Celebrated examples include incommensurate magnetism with long- and short-range magnetic orders [1,2] and Fulde-Ferrell-Larkin-Ovchinnikov (FFLO) pairing states [3,4]. Recently, Bose-Einstein condensations (BECs) with spin-orbit (SO) coupling introduced a new member to this family. The SO coupled BECs are genuinely new phenomena due to the fact that the kinetic energy is not just a Laplacian but also linearly depends on momentum, which gives rise to the complex-valued and even quaternionic-valued condensate wave functions beyond the "no-node" theorem [5,6].

An important property of SO coupled condensates of bosons is that they can spontaneously break time-reversal symmetry, which is impossible in conventional BECs of both superfluid ^{4}He and many experiments of ultracold alkali bosons [7]. For example, it is predicted that such condensates can spontaneously develop a half-quantum vortex coexisting with two-dimensional (2D) skyrmion-type spin textures in the harmonic trap [8]. Experimentally, spin textures of the SO coupled bosons have been observed in exciton condensations, which is a solid-state boson system with relativistic SO coupling [9]. Theoretically, extensive studies have been performed for SO coupled bosons which exhibit various spin orderings and textures arising from competitions among SO coupling, interaction, and confining trap energy [8,10–18].

In the optical lattice, the SO coupled bosons are even more interesting. Early investigations have showed that the characteristic incommensurate wave vectors are incommensurate with the lattice [19]. In this Rapid Communication, we study the SO coupled Bose-Hubbard model, focusing on the magnetic properties. The tight-binding model is constructed and the spin-independent hopping integral t and SO coupled hopping integral λ are calculated as functions of the SO coupling strength in the continuum. Magnetic superexchange models are derived as characterized by the Dzyaloshinsky-Moriya (DM) interaction [20,21]. In the Mott-insulating phase, the single-particle condensation is suppressed but the spin orderings are not. The spin orderings are solved in two different limits, $|\lambda| \ll |t|$ and $|t| \ll |\lambda|$, respectively. In the former case, the DM term destabilizes the ferromagnetic state to spin spirals, while in the latter case, a 2×2 in-plane spin ordering is formed.

We begin with the noninteracting Hamiltonian of bosons with the Rashba SO coupling in a square lattice optical potential as

$$H_0 = \frac{\hbar^2 \mathbf{k}^2}{2m}\hat{1} + \frac{\hbar^2 k_{\rm so}}{m}(\alpha k_x \hat{\sigma}_y + \beta k_y \hat{\sigma}_x) + V(x,y), \quad (1)$$

where $k_{\rm so}$ is the magnitude of wave vectors of laser beams generating SO coupling. α and β characterize the anisotropy of SO coupling. Below we consider two situations. First, SO coupling is only along the x direction, i.e., $\alpha = 1, \beta = 0$, which agrees with the recent experiments [22]. Second, the isotropic Rashba SO coupling with $\alpha = 1, \beta = 1$. $V(x,y)$ is the periodic potential produced by laser beams with wavelength λ_0 as

$$V(x,y) = -V_0[\cos^2 k_0 x + \cos^2 k_0 y], \quad (2)$$

where $k_0 = 2\pi/\lambda_0$, and the recoil energy $E_r = \frac{\hbar^2 k_0^2}{2m}$. We define a dimensionless parameter $\gamma_0 = k_{\rm so}/k_0$ to characterize the strength of SO coupling. The lattice constant $a = \lambda_0/2$, and the reciprocal lattice is $\mathbf{G}_1 = (\frac{2\pi}{a}, 0)$, $\mathbf{G}_2 = (0, \frac{2\pi}{a})$. The band structure of Eq. (1) is calculated by using the plane-wave basis.

In the absence of SO coupling, the two-component bosons with strong optical potentials can be described by the lattice Bose-Hubbard model as

$$H_{\rm Hub} = -\sum_{\langle ij\rangle,\sigma} t_{ij}[b^\dagger_{i,\sigma} b_{j,\sigma} + \text{H.c.}] + \sum_i \left[\frac{U}{2} n_i^2 - \mu n_i\right], \quad (3)$$

where $\sigma = \uparrow, \downarrow$ denote the pseudospin components; $b_{i\sigma}$ and $b^\dagger_{i\sigma}$ are bosonic annihilation and creation operators for spin σ at site i, respectively. $\sum_{\langle i,j\rangle}$ denotes the summation over all the nearest neighbors. n_i is the boson density operator at site i: $n_i = \sum_\sigma b^\dagger_{i\sigma} b_{i\sigma}$. Generally, the interaction can be spin dependent, and we only consider the spin-independent interaction below. A previous study of magnetism of two-component bosons includes Ref. [23], and we will consider it in the presence of SO coupling.

 ©2012 American Physical Society

The case of $\alpha = 1$, $\beta = 0$ is directly related to current experiments in the absence of optical lattice [22]. The SO coupling induces an extra term in the tight-binding term as

$$H_{\rm so} = -\lambda \sum_{\mathbf{i}} \left[b^{\dagger}_{\mathbf{i},\uparrow} b_{\mathbf{i}+\vec{e}_x,\downarrow} - b^{\dagger}_{\mathbf{i},\downarrow} b_{\mathbf{i}+\vec{e}_x,\uparrow} \right] + \text{H.c.}, \tag{4}$$

where $\vec{e}_x$ is the unit vector along the x direction. In momentum space, Eq. (4) becomes $H_{\rm so} = \sum_{\mathbf{k}} \Psi^{\dagger}_{\mathbf{k}} \hat{H}_{\mathbf{k}} \Psi_{\mathbf{k}}$, where $\Psi_{\mathbf{k}} = [b_{\mathbf{k},\uparrow}, b_{\mathbf{k},\downarrow}]^T$, and $\hat{H}^1_{\mathbf{k}}$ is a 2×2 matrix that reads as

$$\hat{H}_{\mathbf{k}} = \varepsilon_{\mathbf{k}} \hat{I} + 2\lambda \sin k_x \hat{\sigma}_y, \tag{5}$$

where $\varepsilon_{\mathbf{k}} = -2(t_x \cos k_x + t_y \cos k_y) - \mu$ and $t_x(t_y)$ is the hopping integrals along the x and y directions, respectively. In the long-wave limit $k \to 0$, Eq. (5) reduces to the Hamiltonian in continuous space realized in experiments.

The SO coupling is equivalent to a pure gauge at $\beta = 0$, which can be eliminated by a gauge transformation

$$U = \exp\{i \mathbf{k}_{\mathbf{so}} \cdot \mathbf{r} \sigma_z\}, \tag{6}$$

which applies to the doublet $(b_\uparrow, b_\downarrow)$. Physically, this gauge transformation corresponds to a local pseudospin rotation by $\theta(\mathbf{r}) = \mathbf{k}_{\mathbf{so}} \cdot \mathbf{r}$ about the pseudospin z axis. The energy spectra of Eq. (5) has two branches as $E_{\pm} = -2t_y[\cos(k_x \pm k_{\rm so}) + \cos k_y] - \mu$, and the following relations are satisfied:

$$t_x = t_y \cos k_{\rm so}, \quad \lambda = t_y \sin k_{\rm so}. \tag{7}$$

Bosons condense into the energy minima of $\pm\mathbf{Q} = (\pm k_1, 0)$ with $k_1 = \arctan(\lambda/t_y)$. The corresponding single-particle wave functions at these two minima are

$$\Psi_{\pm\mathbf{Q}} = \frac{1}{\sqrt{2}} e^{\pm i \mathbf{r}\cdot\mathbf{Q}_{\rm sc}} \begin{pmatrix} 1 \\ \pm i \end{pmatrix}. \tag{8}$$

At the Hartree-Fock level, bosons can take either of $\Psi_{\mathbf{Q}_{\rm sc}}$ as a plane-wave spin-polarized state, or a superposition of them as $\frac{1}{\sqrt{2}}(\Psi_{\mathbf{Q}} + \Psi_{-\mathbf{Q}}) = [\cos \mathbf{Q}\cdot\mathbf{r}, \sin \mathbf{Q}\cdot\mathbf{r}]^T$ with the same energy. The latter one can be stabilized by spin-dependent interaction of $H_{\rm sp,int} = U' \sum (n_{i,\uparrow} - n_{i,\downarrow})^2$ with $U' < 0$. It exhibits a spin spiral states in the xz plane with the pitch wave vector $2\mathbf{Q}$ as plotted in Fig. 1. We will see that in the Mott-insulating state, although a strong interaction suppresses the superfluidity, the spin configuration remains the same spiral order.

We consider the Mott-insulating state at $\langle n_i \rangle = 1$, and construct the superexchange Hamiltonian for the pseudospin-$\frac{1}{2}$ bosons as

$$H_{\rm eff} = \sum_{\mathbf{i}} \left[H_{\mathbf{i},\mathbf{i}+\hat{e}_y} + H_{\mathbf{i},\mathbf{i}+\hat{e}_x} \right]. \tag{9}$$

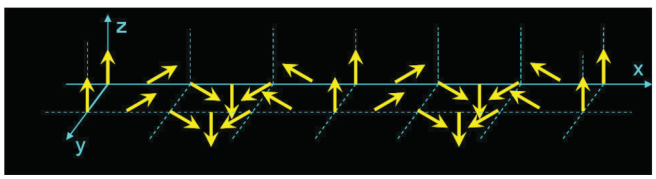

FIG. 1. (Color online) Spin spiral configurations of the Bose-Hubbard model with unidirectional SO coupling. It is valid for both the incommensurate superfluid state, and the Mott insulating state.

For the vertical bond without SO coupling, $H_{i,i+e_y}$ is just the SU(2) ferromagnetic Heisenberg superexchange [24,25] as $H_{\mathbf{i},\mathbf{i}+\hat{e}_y} = -J_{1,y} \mathbf{S}_{\mathbf{i}} \cdot \mathbf{S}_{\mathbf{i}+\hat{e}_y}$, where $J_{1,y} = 4t_y^2/U > 0$. For the horizontal bond, the SO coupling leads to the Dzyaloshinsky-Moriya (DM) type superexchange terms [20,21] as

$$\begin{aligned} H_{\mathbf{i},\mathbf{i}+\hat{e}_x} = & -J_{1,x} \mathbf{S}_{\mathbf{i}} \cdot \mathbf{S}_{\mathbf{i}+\hat{e}_x} - J_{12} \mathbf{d}_{\mathbf{i},\mathbf{i}+\hat{e}_x} \cdot \left(\mathbf{S}_{\mathbf{i}} \times \mathbf{S}_{\mathbf{i}+\hat{e}_x} \right) \\ & + J_2 \left[\mathbf{S}_{\mathbf{i}} \cdot \mathbf{S}_{\mathbf{i}+\hat{e}_x} - 2 \left(\mathbf{S}_{\mathbf{i}} \cdot \mathbf{d}_{\mathbf{i},\mathbf{i}+\hat{e}_x} \right) \left(\mathbf{S}_{\mathbf{i}+\hat{e}_x} \cdot \mathbf{d}_{\mathbf{i},\mathbf{i}+\hat{e}_x} \right) \right], \end{aligned} \tag{10}$$

where $J_2 = 4\lambda^2/U$, $J_{12} = 4t_x\lambda/U$. $\mathbf{d}_{\mathbf{i},\mathbf{i}+\hat{e}_x}$ is a three-dimensional (3D) DM vector defined on the bond $[\mathbf{i}, \mathbf{i}+\hat{e}_x]$ and $\mathbf{d}_{\mathbf{i},\mathbf{i}+\hat{e}_x} = \hat{e}_y$.

The DM term of Eq. (10) prefers a spin spiral ordering along the horizontal direction, as illustrated in Fig. 1. The effect of the gauge transformation Eq. (6) on spin operators is to rotate $\mathbf{S}_{\mathbf{i}}$ around the y axis at the angle of $2m\theta$, where m is the horizontal coordinate of site i and $\theta = \arctan(\lambda/t_x)$ [26], such that

$$\mathbf{S}'_{\mathbf{i}} = (1 - \cos 2m\theta)[\mathbf{d} \cdot \mathbf{S}_{\mathbf{i}}]\mathbf{d} + \cos 2m\theta \mathbf{S}_{\mathbf{i}} - \sin 2m\theta \mathbf{S}_{\mathbf{i}} \times \mathbf{d}, \tag{11}$$

where $\mathbf{d} = \mathbf{d}_{\mathbf{i},\mathbf{i}+\hat{e}_x} = \hat{e}_y$. Through this transformation, the DM interaction is gauged away, and Eq. (10) turns into a ferromagnetic coupling:

$$H_{\mathbf{i},\mathbf{i}+\hat{e}_x} = -J_0 \mathbf{S}'_{\mathbf{i}} \cdot \mathbf{S}'_{\mathbf{i}+\hat{e}_x}, \tag{12}$$

where $J_0 = J_{1,x} = 4(t_x^2 + \lambda^2)/U$. The exchange model becomes an isotropic ferromagnetic Heisenberg model, and thus spin polarization can point along any direction. In order to obtain the actual spin spiral configuration, we need to do the inverse operation of Eq. (11). Say if we choose the classic spin at the point of origin along z direction $\mathbf{S}_{[0,0]} = \hat{e}_z$, according to the rotation defined in Eq. (11), all the spins in the classic ground state are restricted within the x-z plane, and the classic spin at the point $[m,n]$ is $\mathbf{S}_{[m,n]} = \cos(2m\theta)\hat{e}_z + \sin(2m\theta)\hat{e}_x$. As shown in Fig. 1(b), the classic spins form a chiral pattern with a characteristic length, which is the same as in the superfluid case as plotted in Fig. 1. The only difference is that the superfluid phase coherence is lost in the Mott-insulating state.

Now we discuss the isotropic Rashba SO coupling with $\alpha = \beta = 1$. From the symmetry analysis, we easily have $t_x = t_y$ for spin-independent hoppings, while the spin-dependent SO hoppings become

$$\begin{aligned} H'_{\rm so} = & -\lambda \sum_{\mathbf{i}} \left[b^{\dagger}_{\mathbf{i},\uparrow} b_{\mathbf{i}+\vec{e}_x,\downarrow} - b^{\dagger}_{\mathbf{i},\downarrow} b_{\mathbf{i}+\vec{e}_x,\uparrow} \right] + \text{H.c.}, \\ & - i\lambda \sum_{\mathbf{i}} \left[b^{\dagger}_{\mathbf{i},\downarrow} b_{\mathbf{i}+\vec{e}_y,\uparrow} + b^{\dagger}_{\mathbf{i},\uparrow} b_{\mathbf{i}+\vec{e}_y,\downarrow} \right] + \text{H.c.} \end{aligned} \tag{13}$$

In momentum space, the tight-binding band Hamiltonian becomes $H' = \sum_{\mathbf{k}} \Psi^{\dagger}_{\mathbf{k}} \hat{H}'_{\mathbf{k}} \Psi_{\mathbf{k}}$, where

$$\hat{H}'_{\mathbf{k}} = \varepsilon_{\mathbf{k}} \hat{I} + 2\lambda [\sin k_x \hat{\sigma}_y + \sin k_y \hat{\sigma}_x], \tag{14}$$

where $\varepsilon_{\mathbf{k}} = -2t(\cos k_x x + \cos k_y y)$. The energy spectra of Eq. (14) read

$$E'_{\pm} = \varepsilon_{\mathbf{k}} \pm 2\lambda \sqrt{\sin^2 k_x + \sin^2 k_y}. \tag{15}$$

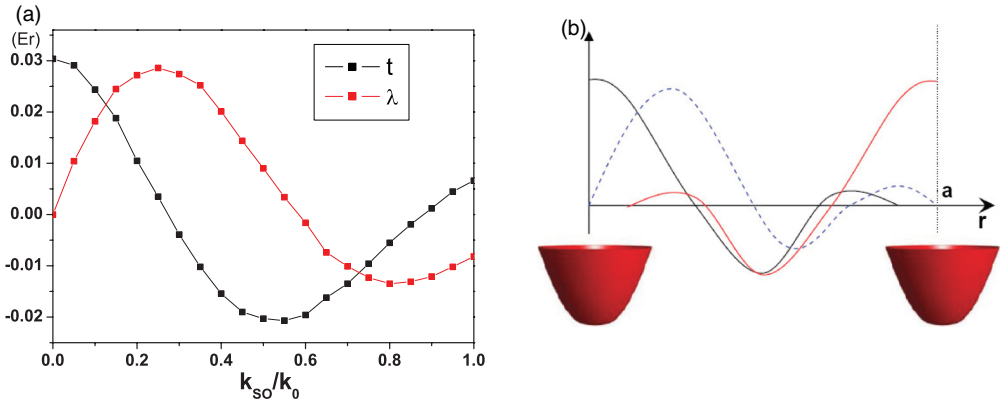

FIG. 2. (Color online) (a) The dependence of the spin-independent hopping integral t and the spin-dependent one λ vs the SO coupling strength $\gamma = k_{so}/k_0$. The optical potential depth is $V_0 = 8E_r$. (b) Sketch of Wannier wave functions for $f(r)$ (solid black line), $f(r-a)$ (solid red line), and $g(r)$ (dashed blue line) in Eq. (16), where a is the lattice constant.

The band minima are fourfold degenerate at the points $\mathbf{Q}_{sc} = (\pm k, \pm k)$, where $k = \arctan \frac{\lambda}{\sqrt{2}t}$.

Next we calculate the band parameters t and λ versus the SO coupling parameter γ by fitting the band spectra using the plane-wave basis in the continuum. The results are plotted in Fig. 2(a). Both t and λ oscillate and decay with increasing γ, which can be understood from the behavior of the on-site Wannier functions. Each optical site can be viewed as a local harmonic potential and the lowest single-particle state wave function was calculated in Ref. [8],

$$\psi_{j_z=\frac{1}{2}}(\vec{r}) = [f(r), g(r)e^{i\phi}]^T, \tag{16}$$

and its time-reversal partner is $\psi_{j_z=-\frac{1}{2}}(\vec{r}) = [-g(r)e^{i\phi}, f(r)]$. $f(r)$ and $g(r)$ are real radial wave functions, which exhibit characteristic oscillations with the pitch value k_{so} and a relative phase shift approximately $\frac{\pi}{2}$ as plotted in Fig. 2(b). t and λ are related to the off-centered integrals of $f(r)$ and $g(r)$ of two sites, which overlap in the middle. As a result, t and λ also oscillate as increasing γ, which also exhibit a phase shift approximately at $\pi/2$ as shown in Fig. 2(a).

We would like to clarify one important and subtle point. Actually the on-site Wannier functions are no longer spin eigenstates, but the total angular momentum eigenstate $j_z = \frac{1}{2}$, and thus are still a pair of Kramer doublets. For the operators $(b_{i\uparrow}, b_{i,\downarrow})^T$ defined on site i, they do not refer to spin eigenbasis but to the j_z eigenbasis. In fact, in the case that $k_{so} \geqslant k_0$, the on-site spin moments are nearly zero. The j_z movements mainly come from an orbital angular momentum. As pointed out in Ref. [8], the Wannier functions of j_z eigenstates exhibit skyrmion-type spin texture distributions and a half-quantum vortex on each site. This phenomena also remind us of the Friedel oscillation in solid-state physics. In the case of $k_{so} \gg k_0$, each site exhibits Landau level-type quantization: States with different values of j_z are nearly degenerate [8,18], and a single band picture ceases to work here.

Deep inside the Mott-insulating phase, we obtain the effective magnetic Hamiltonian:

$$H'_{\text{eff}} = \sum_{\mathbf{i}} \left[H'_{\mathbf{i},\mathbf{i}+\hat{e}_y} + H'_{\mathbf{i},\mathbf{i}+\hat{e}_x} \right]. \tag{17}$$

$H'_{\mathbf{i},\mathbf{i}+\hat{e}_x}$ is the same as Eq. (10), and

$$\begin{aligned} H'_{\mathbf{i},\mathbf{i}+\hat{e}_y} = & -J_1 \mathbf{S}_{\mathbf{i}} \cdot \mathbf{S}_{\mathbf{i}+\hat{e}_y} - J_{12} \mathbf{d}_{\mathbf{i},\mathbf{i}+\hat{e}_y} \cdot \left(\mathbf{S}_{\mathbf{i}} \times \mathbf{S}_{\mathbf{i}+\hat{e}_y} \right) \\ & + J_2 \left[\mathbf{S}_{\mathbf{i}} \cdot \mathbf{S}_{\mathbf{i}+\hat{e}_y} - 2 \left(\mathbf{S}_{\mathbf{i}} \cdot \mathbf{d}_{\mathbf{i},\mathbf{i}+\hat{e}_y} \right) \left(\mathbf{S}_{\mathbf{i}+\hat{e}_y} \cdot \mathbf{d}_{\mathbf{i},\mathbf{i}+\hat{e}_y} \right) \right], \end{aligned} \tag{18}$$

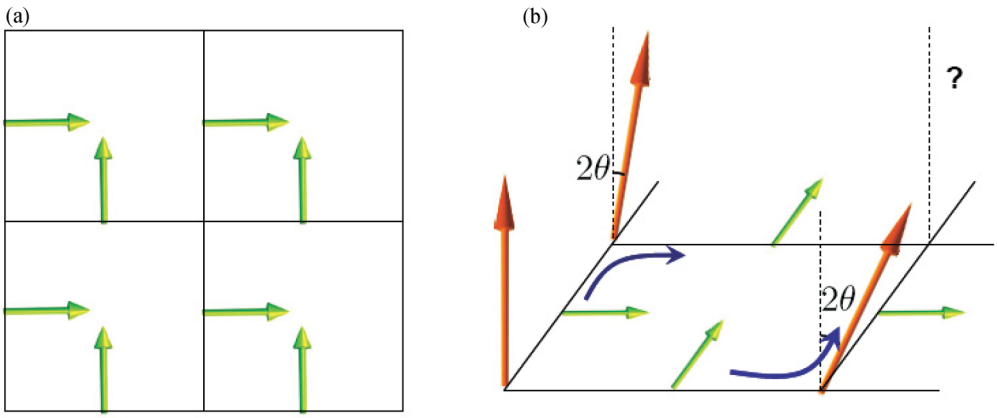

FIG. 3. (Color online) (a) The pattern of DM vectors of the superexchange magnetic model in the Mott-insulating state. (b) Illustration of the frustration in the spin configuration with DM interactions; the rotations around the x and y axes do not commutate with each other.

where $\mathbf{d}_{\mathbf{i},\mathbf{i}+\hat{e}_y} = \hat{e}_x$. The pattern of the DM vectors is shown in Fig. 3(a), which is strongly reminiscent of that in the cuprate superconductor $YBa_2Cu_3O_6$ [27,28]. The classical ground state of Eq. (17) is nontrivial because the DM interaction cannot be gauged away: DM vectors in horizontal bonds favor spiraling around the y axis, while those in vertical bonds favor spiraling around the x axis. Since rotations around the x and y axes do not commune, no spin configurations can simultaneously satisfy both requirements, which leads to spin frustrations shown in Fig. 3(b).

The quantum situation of Eq. (17) is even more involved, which can only be solved approximately. Below we focus on two situations: $|\lambda| \ll |t|$ and $|\lambda| \gg |t|$. At $\lambda = 0$, the ground state of Eq. (17) is known to be ferromagnetic. At $|\lambda/t| \ll 1$, we use a spin-wave approximation to analyze the instability of a ferromagnetic state induced by the DM interaction. Notice that in this case, it is impossible to find a global rotation as in Eq. (11) to gauge away the DM vectors and transform Eq. (17) to an SO(3) invariant Hamiltonian, and thus the quantized axis in the spin-wave analysis cannot be chosen arbitrarily. To gain some insight, we choose a classic ferromagnetic state as a variational ground state parametrized by $\mathbf{S_i} = S(\cos\gamma \sin\eta, \sin\gamma \sin\eta, \cos\eta)$. The corresponding variational energy $E_0 = -S^2(J_1 - J_2 + 2\sin^2\eta J_2)$ is minimized when $\eta = \pi/2$, which implies that the xy plane is the easy plane.

To calculate the spin-wave spectra, it is convenient to rotate the coordinate so that the new z-axis points along the direction $\mathbf{l} = [\bar{1}\bar{1}0]$ in the original coordinate (we choose $\mathbf{l}$ as the quantized axis). The Holstein-Primakoff transformation is employed to transform Eq. (17) into the bosonic Hamiltonian:

$$H_b = \sum_{i,\mu} -J_0(\cos 2\theta - i \sin 2\theta/\sqrt{2}) a_i^\dagger a_{i+e_\mu} + \text{H.c.}, \qquad (19)$$

where $\theta = \arctan(\lambda/t)$ as defined above, $\mu = x, y$. We only keep quadric terms and ignore the terms proportional to $\sin^2\theta$ since $\lambda/t \ll 1$. In momentum space, it becomes

$$H'_{\text{ex}} = -2J_0 \sum_{\mathbf{k}} \Big[\cos 2\theta \cos k_x + \frac{1}{\sqrt{2}} \sin 2\theta \sin k_x + \cos 2\theta \cos k_y + \frac{1}{\sqrt{2}} \sin 2\theta \sin k_y \Big] c_{\mathbf{k}}^\dagger c_{\mathbf{k}}. \qquad (20)$$

The minimum of the dispersion of Eq. (20) occurs at points $\mathbf{Q}_M = (\pm k', \pm k')$, where k' satisfies $\tan k' = \frac{1}{\sqrt{2}} \tan 2\theta$. Comparing it with the energy minima in the noninteracting band Hamiltonian $\mathbf{Q}_{sf} = (\pm k, \pm k)$, we have $k' = 2k$ at the limit of $\gamma \to 0$. The nonzero minimum of the magnon spectrum is a signature of the spin spiral order, as shown in Fig. 4(a).

In the opposite limit of $|\lambda/t| \gg 1$, if we consider the Eq. (17) as a classic Hamiltonian, the J_2 term has a continuous degenerate manifold. The DM J_{12} energy is zero for all of them, and thus does not lift the degeneracy. The ferromagnetic coupling J_1 term selects the configuration of spin lying on the xy plane with the 2×2 pattern shown in Fig. 4(b). This is a discrete symmetry-breaking state, and thus there is no Goldstone mode for these 2×2 states. The magnon excitation should be gapped even at a quantum level, and such a state is stable at large values of λ/t. For the intermediate values of λ/t, we expect quantum phase transitions from the spin spiral state in Fig. 4(a) to the 2×2 state in Fig. 4(b). Due to the very different spin configurations, rich phase structures with exotic patterns of spin spirals and textures are expected.

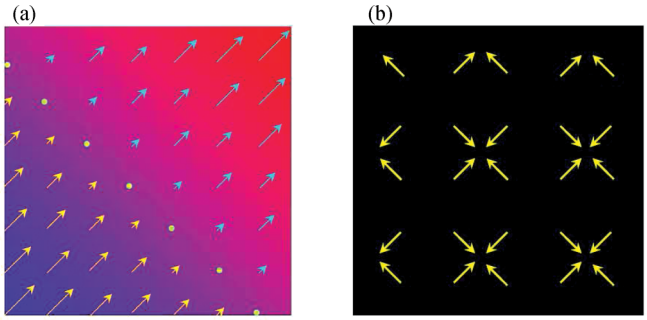

FIG. 4. (Color online) (a) Spin spiral ordering in the limit of $|\lambda| \ll |t|$. (b) The 2×2 pattern in limit of $|t| \ll |\lambda|$.

The magnetic orders proposed above can be detected by the spin-dependent Bragg scattering. The transition rate for the elastic Bragg scattering is directly related to the spin structure factor for the atoms, and thus will exhibit a peak in the characteristic momentum $\mathbf{Q}$ of the spin spiral states. Similar methods have been proposed to detect the antiferromagnetic state [29] as well as the FFLO state [24,25,30] in cold atoms.

In conclusion, we have investigated the magnetic ordering of a two-component Bose-Hubbard model with synthetic SO coupling. The band parameters of hopping integrals exhibit characteristic oscillations with increasing SO coupling strength, and the on-site magnetic moments are nearly orbital moments at large SO coupling strength. In the Mott-insulating state with one particle per site, an effective magnetic superexchange model with the DM-type interaction is derived. The spin spiral state and the 2×2 states are found in the limits of $|\lambda| \ll |t|$ and $|\lambda| \gg |t|$, respectively.

Recently, we become aware two papers on the similar topic [31,32]. We also recently became aware of Ref. [33].

This work was supported in part by the NBRPC (973 program) 2011CBA00300 (2011CBA00302), and DMR-1105945. We acknowledge financial support from a AFOSR-YIP award.

[1] N. Read and S. Sachdev, Phys. Rev. Lett. **66**, 1773 (1991).
[2] S. Sachdev and N. Read, Mod. Phys. Lett. **5**, 219 (1991).
[3] P. Fulde and R. A. Ferrell, Phys. Rev. **135**, A550 (1964).
[4] A. I. Larkin and Y. N. Ovchinnikov, Sov. Phys. JETP **20**, 762 (1965).
[5] R. P. Feynman, *Statistical Mechanics, A Set of Lectures* (Addison-Wesley, Berlin, 1972).
[6] C. Wu, Mod. Phys. Lett. B **20**, 1707 (2006); Y. Li, X. F. Zhou, and C. Wu, arXiv:1205.2162.
[7] A. J. Leggett, Rev. Mod. Phys. **73**, 307 (2001).

[8] C. Wu, I. Mondragon-Shem, and X. F. Zhou, Chin. Phys. Lett. **28**, 097102 (2011).
[9] A. A. High *et al*., Nature (London) **483**, 584 (2012).
[10] T. D. Stanescu, B. Anderson, and V. Galitski, Phys. Rev. A **78**, 023616 (2008).
[11] T.-L. Ho and S. Zhang, Phys. Rev. Lett. **107**, 150403 (2011).
[12] C. Wang, C. Gao, C. M. Jian, and H. Zhai, Phys. Rev. Lett. **105**, 160403 (2010).
[13] S.-K. Yip, Phys. Rev. A **83**, 043616 (2011).
[14] Y. Zhang, L. Mao, and C. Zhang, Phys. Rev. Lett. **108**, 035302 (2012).
[15] X.-F. Zhou, J. Zhou, and C. Wu, Phys. Rev. A **84**, 063624 (2011).
[16] Y. Li, X. F. Zhou, and C. Wu, arXiv:1205.2162.
[17] S. Gopalakrishnan, A. Lamacraft, and P. M. Goldbart, Phys. Rev. A **84**, 061604(R) (2011).
[18] H. Hu, B. Ramachandhran, H. Pu, and X. J. Liu, Phys. Rev. Lett. **108**, 010402 (2012).
[19] I. Mondragon-shem, B. A. Rodriguez, and C. Wu, Bull. Am. Phys. Soc. **55**, Z31.11 (2010); I. Mondragon-shem, Bachelor thesis, Instituto de Física, Facultad de Ciencias Exactas y Naturales, Universidad de Antioquia, 2010.
[20] I. Dzyaloshinsky, J. Phys. Chem. Solids **4**, 241 (1958).
[21] T. Moriya, Phys. Rev. **120**, 91 (1960).
[22] Y.-J. Lin, K. Jiménez-García, and I. B. Spielman, Nature (London) **471**, 83 (2011).
[23] A. Isacsson, M.-C. Cha, K. Sengupta, and S. M. Girvin, Phys. Rev. B **72**, 184507 (2005); T. Grass, K. Saha, K. Sengupta, and M. Lewenstein, Phys. Rev. A **84**, 053632 (2011).
[24] L. M. Duan, E. Demler, and M. D. Lukin, Phys. Rev. Lett. **91**, 090402 (2003).
[25] A. B. Kuklov and B. V. Svistunov, Phys. Rev. Lett. **90**, 100401 (2003).
[26] L. Shekhtman, O. Entin-Wohlman, and A. Aharony, Phys. Rev. Lett. **69**, 836 (1992).
[27] D. Coffey, T. M. Rice, and F. C. Zhang, Phys. Rev. B **44**, 10112 (1991).
[28] N. E. Bonesteel, Phys. Rev. B **47**, 11302 (1993).
[29] T. A. Corcovilos, S. K. Baur, J. M. Hitchcock, E. J. Mueller, and R. G. Hulet, Phys. Rev. A **81**, 013415 (2010).
[30] R. M. Lutchyn, M. Dzero, and V. M. Yakovenko, Phys. Rev. A **84**, 033609 (2011).
[31] J. Radic, A. Di Ciolo, K. Sun, and V. Galitski, arXiv:1205.2110.
[32] W. S. Cole, S. Z. Zhang, A. Paramekanti, and N. Trivedi, arXiv:1205.2319.
[33] S. Mandal, S. Mandal, K. Saha, and K. Sengupta, arXiv:1205.3178; M. Gong, Y. Qian, V. W. Scarola, and C. W. Zhang, arXiv:1205.6211.